Desalination and Water Treatment
www.deswater.com

doi: 10.1080/19443994.2014.994104

57 (2016) 4681–4693
February

Taylor & Francis
Taylor & Francis Group

Modification and use of biochar from wheat straw (*Triticum aestivum* L.) for nitrate and phosphate removal from water

Ji-hui Li[a], Guo-hua Lv[a], Wen-bo Bai[a], Qi Liu[a,c], Yuan-cheng Zhang[b], Ji-qing Song[a,*]

[a]*State Key Engineering Laboratory of Crops Efficient Water Use and Drought Mitigation, Institute of Environment and Sustainable Development in Agriculture, Chinese Academy of Agricultural Sciences, No. 12 South Street Zhongguancun, Beijing 100081, China, Tel./Fax: +86 10 82109764; email: songjiqing@caas.cn (J.-q. Song)*
[b]*Baoli Biomass Energy Joint Stock Company Limited, Changan Group (Shengli Oilfield), Dongying 257067, China*
[c]*Department of Agriculture, Bio-Engineering and Chemistry, University of Liege-Gembloux Agro-Bio Tech, Gembloux 5030, Belgium*

Received 8 April 2014; Accepted 26 November 2014

ABSTRACT

Surface modification can improve biochar adsorption capacity. Biochars were produced from wheat straw through low-temperature pyrolysis at approximately 450°C, activated with hydrochloric acid (HCl), and coated with iron ($FeCl_3{\cdot}6H_2O$) of different amounts. Results showed that activation with HCl and coating with iron can significantly increase biochar adsorption capacity. The increase after HCl treatment was very small at a high ratio of iron to biochar. The optimal ratio of iron to biochar for iron-coated biochar was 0.70. Adsorption capacity was calculated based on the amount of pure nitrogen or phosphorus. The maximum adsorption capacities were 2.47 and 16.58 mg g^{-1}. The most effective pH values for nitrate and phosphate removal were 3 and 6, respectively. The active substance of the optimal-modified biochar (OMB) was amorphous FeOOH, and the structure $[C–Fe(OH_2)_5]^{3+}_{(s)}$ was the hydroxylated mineral surface of OMB in a water solution. The equilibrium pH of the adsorption solution was lower than 7 even when the initial pH of the solution was 11 because $[C–Fe(OH_2)_5]^{3+}_{(s)}$ changed into $[C–Fe(OH_2)_4(OH)]^{2+}_{(s)}$, $[C–Fe(OH_2)_3(OH)]^{+}_{(s)}$, and H_3O^+ with the increase in pH. Adsorption experiments showed that OMB can be utilized to remove nitrate and phosphate from water.

Keywords: Nitrate removal; Phosphate removal; Wheat straw biochar; Iron-coated biochar

1. Introduction

Millions of tons of agricultural bioresources, such as wheat straw, have been produced by agriculture in China in recent years. Several researchers have estimated that 110–157.5 Tg of crop wastes are burned in fields every year; this activity releases a large amount of pollutants into the atmosphere, including particulate matter, CO, and hydrocarbons [1]. As a result, the environment becomes polluted, and bioresources are wasted. As a type of natural resource, wheat straw can be utilized to prepare biochar for extensive applications.

Biochar, a carbon-rich solid byproduct of the pyrolysis of biomass under the complete exclusion of oxygen at temperatures below 700°C [2–4], can be derived from a large range of low-cost biomass sources, including manure, organic wastes, bioenergy crops (e.g. grasses and willows), and crop residues [4].

*Corresponding author.

Many studies have applied biochar to soil because of its high resistance to decay and excellent capability to retain nutrients [4]. Biochar can also mitigate climate change, improve soil quality, and reduce environmental pollution [4–7]. In addition to its application to soil, a number of studies have utilized biochar as a highly efficient and low-cost adsorbent in wastewater treatment to remove different types of pollutants. Many different biomass-derived biochars have been proposed for the removal of organic contaminants [8–11], heavy metals [12,13], and nutrient pollutants [9] from water.

Raw wheat straw biochar has a very low adsorption capacity for nitrate and phosphate because of its large negative surface charge [4]; moreover, its loose texture and low density make it difficult to disperse in a water solution. A good method is necessary to increase the adsorption capacity and fully maximize the use of this raw material. Previous studies have shown that adsorption capacity can be improved through several surface modification techniques. One of these techniques is to activate the surface of the adsorbent with an acid, such as hydrochloric acid (HCl). After activation, the pores of the adsorbent particles become more heterogeneous than those of the raw particles, which mean that more activated sites become available [14]. Moreover, treatment of adsorbents with acid produces more positive sites on the surface of the adsorbent, and protonation of surface hydroxyl groups causes an increase in the electrostatic adsorption of anions, such as nitrate [15]. Another method is to introduce metal (hydr)oxides, mainly iron (hydr)oxides, into porous carbon-rich adsorbents, such as biochar or activated carbon. Iron (hydr)oxides, such as goethite, haematite, ferrihydrite, and akaganeite, can be produced by the precipitation of ferric salts and occur naturally in mineral forms. The products, however, have varying chemical and physical properties, such as structure, composition, surface area, morphology, and color, because of the use of different preparatory techniques [16]. Iron (hydr)oxides have a high affinity toward oxy-anion ions, such as arsenate and phosphate, and are very selective in the adsorption process [17,18]. The mechanisms for arsenate and phosphate removal are adsorption onto iron (hydr) oxide surfaces and formation of ferric arsenate and ferric phosphate. Several researchers have found that the biochar adsorption capacities of some pollutants, including arsenic [19] and phosphorus [20], are higher than that of the raw material after the pollutants have been coated with iron (hydr)oxide.

The objective of this study is to develop a method to increase wheat straw biochar adsorption capacity through surface modification and apply the method to nitrate and phosphate removal from water. Biochar was activated with hydrochloric acid (HCl) and coated with iron ($FeCl_3{\cdot}6H_2O$). The effect of the impregnation mass ratio of iron to biochar on nitrogen and phosphorus adsorption capability was investigated. The optimal ratio, largest adsorption capability, and ideal pH were determined.

2. Materials and methods

2.1. Materials

2.1.1. Biochar production

Wheat straw biochars (WB) were prepared from wheat straws through low-temperature pyrolysis at approximately 450°C [4]. The WB samples were milled and screened, and biochars that were less than 1 mm in size were selected for use. These samples had a bulk density of 0.39 g cm^3 and pH (H_2O) of 8.3. The element contents are shown in Table 1.

2.1.2. Biochar activation

All chemicals were of analytical reagent grade, and the solutions were prepared with distilled water. The WB samples were activated with distilled water, 1 mol L^{-1} hydrochloric acid (HCl) solution, or 6 mol L^{-1} HCl solution. The WB samples (100 g) were soaked in one of these three solutions for 1 h and marked as DWB, 1HWB, and 6HWB. The samples were then washed until the pH of the washed water was 7.0. Afterward, the samples were dried at 75°C for 12 h.

2.1.3. Preparation of iron-coated biochars (IBs)

Exactly 10 g each of DWB, 1HWB, and 6HWB was mixed with 1 mol L^{-1} $FeCl_3$ ($FeCl_3{\cdot}6H_2O$) solution. The volumes of the mixed solutions were 25, 50, 80, 125, and 150 ml, and the corresponding iron content was

Table 1
Elemental analysis (wt%) for wheat straw, biochars, and DIBs

Samples	C	N	C/N	O	H	P	K
Wheat Straw	43.06	0.58	74	36.33	5.72	0.25	1.06
WB	47.20	1.09	43	18.36	2.39	0.69	0.71
6HWB	47.93	1.12	43	17.84	2.50	0.08	0.57
DIB2	25.91	0.62	42	21.60	1.70	0.11	4.88
DIB4	27.14	0.50	54	22.14	1.96	0.16	5.57
DIB5	17.29	0.38	45	24.24	2.21	0.29	4.30

1.4, 2.8, 4.5, 7.0, and 8.4 g, respectively; these values indicate that the mass ratio of iron to biochar in the mixed solutions was 0.14, 0.28, 0.45, 0.70, and 0.84, respectively. The pH of the mixed solutions was adjusted to 7.0 with 3 mol L^{-1} KOH. The mixed solutions were left to stand for 1 h and then, washed with distilled water several times and dried at 75°C. Three series of iron-coated biochars (IBs) were obtained with the solutions and marked as DIBs (DIB1, DIB2, DIB3, DIB4, and DIB5), 1HIBs (1HIB1, 1HIB2, 1HIB3, 1HIB4, and 1HIB5), and 6HIBs (6HIB1, 6HIB2, 6HIB3, 6HIB4, and 6HIB5).

2.2. Methods

2.2.1. Characterization of biochars and IBs

Elemental (C, H, O, and N) analyses were performed with an elemental analyzer (vario PYRO cube, Isoprime Ltd, Elementar Analysensysteme GmbH), and C, H, O, and N levels were measured as CO_2, H_2O, and N_2 gases through high-temperature catalyzed combustion followed by infrared detection. Phosphates and potassium ions were determined by molybdenum antimony ascorbic acid colorimetry and flame photometry after acid digestion, respectively.

The powder morphology and the structure and surface characteristics of the adsorbents before and after activation and iron coating were obtained with a Hitachi Su 8000 Series scanning electron microscope (SEM). Surface element analysis of the IBs (DIB2, DIB4, and DIB5) was performed simultaneously through energy-dispersive X-ray spectrometry (EDS) via the spectroscope attached to the SEM.

The specific surface areas (S_{BET}) of the adsorbents (WB, 6HWB, DIB2, DIB4, and DIB5) were determined through the Brunauer–Emmett–Teller (BET) method via N_2 adsorption at 77 K and with the use of a surface area and porosity analyzer (Micromeritics TriStar II 3020). Total pore volume (V_T) was defined as the volume of liquid nitrogen corresponding to the amount adsorbed at a relative pressure of $P\,P_0^{-1}$ = 0.99. Pore size distribution was determined through the Barrett–Joyner–Halenda (BJH) method, and adsorption average pore width was determined according to the relationship 4 V_T/S_{BET}.

2.2.2. Nitrate and phosphate adsorption

To test the nitrate and phosphate adsorption capacities of DWB, 1HWB, 6HWB, DIBs, 1HIBs, and 6HIBs, 0.6 and 0.2 g of these adsorbents were placed in capped conical flasks containing 50 ml of KNO_3 solution (50 mg N L^{-1}) and 50 ml of KH_2PO_4 solution (50 mg P L^{-1}), respectively, at pH 7.0. The flasks were shaken with a shaker at 100 rpm for 3 h at room temperature. Preliminary study suggests that 3 h is required to reach nitrogen and phosphorus adsorption equilibrium. After 3 h of adsorption, the concentrations of nitrogen and phosphorus were determined via phenol disulfonic acid method and molybdenum antimony ascorbic acid colorimetry, respectively, and the measurements were conducted at wavelengths of 420 and 700 nm, respectively. Each experiment was replicated thrice.

The amount of nitrogen and phosphorus adsorbed onto the adsorbents was calculated with the equation

$$\mathrm{qe} = (C_0 - C_e)\frac{V}{m} \tag{1}$$

where C_0 and C_e (mg L^{-1}) are the initial and equilibrium solution concentrations, respectively; V is the volume of the solution (L); qe (mg g^{-1}) is the amount adsorbed; and m is the weight of each adsorbent used (g).

The removal percentage of nitrogen and phosphorus from aqueous solutions was calculated with the equation below.

$$\text{Removal } (\%) = \frac{(C_0 - C_e)}{C_0} \times 100 \tag{2}$$

2.2.3. Study of the equilibrium adsorption of optimal modified biochar (OMB)

To investigate the equilibrium adsorption of OMB, 0.6 g samples were mixed with 50 ml solutions containing various nitrate concentrations (5, 7, 10, 15, 20, 30, 40, and 50 mg N L^{-1}). Then, 0.2 g samples were mixed with 50 ml solutions containing various phosphate concentrations (40, 50, 60, 70, 80, 90, and 100 mg P L^{-1}). The amount of nitrogen and phosphorus adsorbed was calculated with Eq. (1).

2.2.4. Effect of initial pH on the adsorption capacity of OMB

The pH values of the KNO_3 and KH_2PO_4 solutions (the concentration of nitrogen and phosphorus was 50 mg L^{-1}) were adjusted to different values between 3 and 11. The initial pH of the solution was adjusted with HCl or KOH and a pH meter. IB (0.6 and 0.2 g samples) was added to the 50 ml KNO_3 and KH_2PO_4 solutions. The adsorption of nitrogen and phosphorus was determined with Eq. (1).

2.2.5. Statistical analysis

The nitrogen and phosphorus adsorption capacities of DWB, 1HWB, 6HWB, DIBs, 1HIBs, and 6HIBs were analyzed through one-way analysis of variance (ANOVA) to determine OMB. The means were compared through least significant difference method, and statistical analysis was performed with SAS 9.2.

3. Results and discussion

3.1. Characterization of biochars and IBs

Elemental analysis of wheat straw showed that the residues of agricultural production are carbon-rich materials and have a carbon content of 43.06% (Table 1). The carbon content of wheat straw is only slightly lower than that of WB. After activation with HCl, 6HWB obtained a higher content of carbon, nitrogen, and hydrogen than WB but a lower content of oxygen, phosphorus, and potassium. The higher hydrogen content of 6HWB compared with that of WB suggests that protonation of hydroxyl groups occurred at the surface of 6HWB, which was favorable to the adsorption process. After coating with iron, the carbon content of DIBs decreased more rapidly than that of WB with the increase in the iron (hydr)oxides introduced into the pores of WB. More oxygen, hydrogen, and potassium elements appeared because of the introduced iron (hydr)oxides. Furthermore, the oxygen and hydrogen content of IBs increased as the mass ratio of iron to biochar increased.

The SEM images of WB and 6HWB show that the pores of 6HWB are more regular and heterogeneous than those of WB (Fig. 1). Fig. 2 shows the SEM images of DIB2, DIB4, and DIB5. The EDS spectra of the DIB2, DIB4, and DIB5 surfaces (Fig. 2) show that the pores of these DIBs were coated with plenty of iron (hydr)oxides particles; DIB5 was coated more than DIB4 and DIB2 at low mass ratios. DIB5 had more oxygen and less carbon content, and this finding is in agreement with that of the element analysis (Table 1). These results suggest that WB activation with HCl and iron (hydr)oxide coating leads to the generation of more available activated sites on the surface of the adsorbents for nitrate and phosphate adsorption [14].

The N_2 adsorption–desorption isotherms for WB, 6HWB, DIB2, DIB4, and DIB5 are shown in Fig. 3(a), and the textural characteristics of these adsorbents are listed in Table 2. The isotherm of 6HWB presented a higher adsorption than that of WB and had a larger surface area and pore volume (Table 2). DIB2, DIB4, and DIB5 had a higher N_2 adsorption volume than WB and 6HWB for the total range of relative pressure as well as a larger surface area and pore volume (Table 2). DIB4 had a larger surface area and pore volume than the other adsorbents. These results indicate that an adsorbent may have an increased adsorption capacity for nitrate and phosphate after activation with HCl and iron (hydr)oxide coating, hence the higher adsorption capacity of DIB4 compared with the other adsorbents. The adsorption curves of WB, 6HWB, and DIB2 increased again when the relative pressure was higher than 0.9; however, that of DIB2 increased more gradually than those of WB and 6HWB. These isotherms are classified as type II according to IUPAC. However, this increase was not observed in DIB4 and DIB5 (Fig. 3(a)); these two isotherms are classified as type I which is known as Langmuir. When the relative pressure was higher than 0.4, the desorption curves of DIB2, DIB4, and DIB5 presented a hysteresis loop of type H_4.

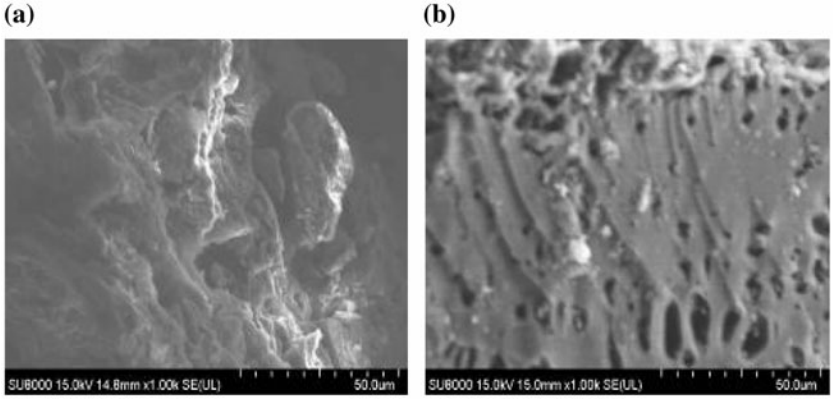

Fig. 1. SEM images of WB (a) and 6HWB (b).

Pore size distribution was determined through BJH method (Fig. 3(b)). The pore structures of the adsorbents were basically micropore and mesopore (smaller than 10 nm). After iron (hydr)oxide coating, the adsorbent acquired a larger pore volume; this value increased initially and then decreased as the amount of coated iron increased (Table 2). These results indicate that the adsorption capacity of DIB4 may be higher than that of the other adsorbents.

3.2. Nitrate adsorption

The removal percentage and amount of adsorbed nitrogen in 1HWB and 6HWB were significantly higher than that in DWB (Fig. 4(a) and Table 3) and increased approximately more than 12 times for 1HWB and 22 times for 6HWB. Furthermore, treating WB with HCl provided the adsorbents a higher surface area and pore volume (Table 2), and may have

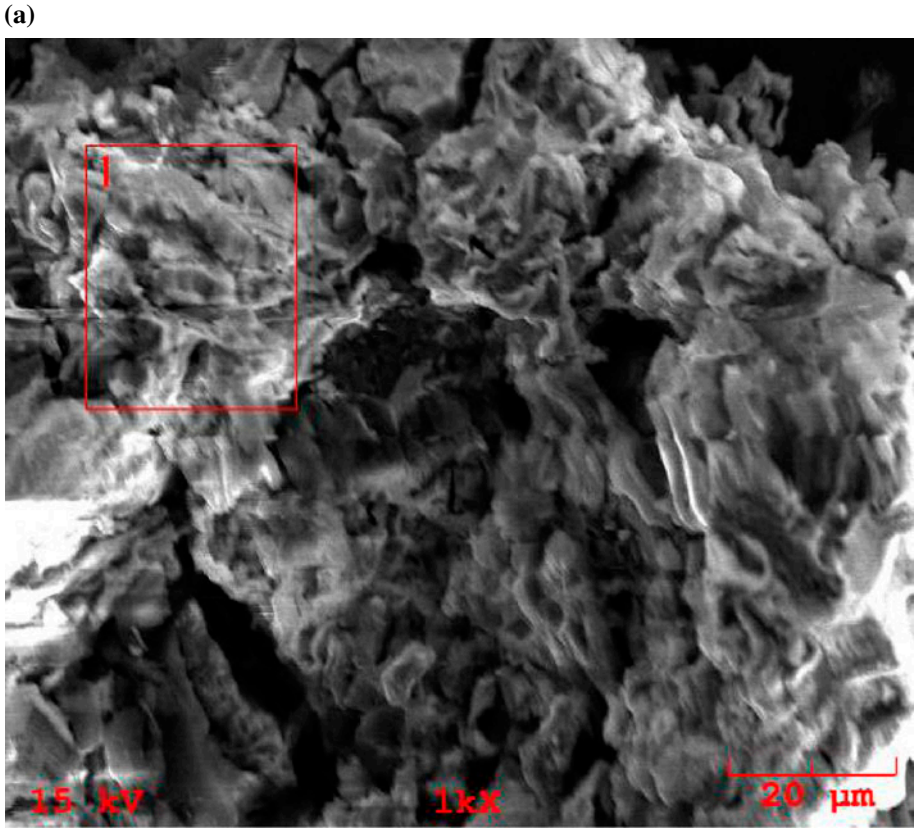

Element	Atomic %	Mass %
C	40.30	25.52
O	42.40	35.76
Fe	8.47	24.95
Total	100	100

Fig. 2. SEM images (upper) and attached EDS spectra (lower) of DIB2 (a), DIB4 (b), and DIB5 (c).

(b)

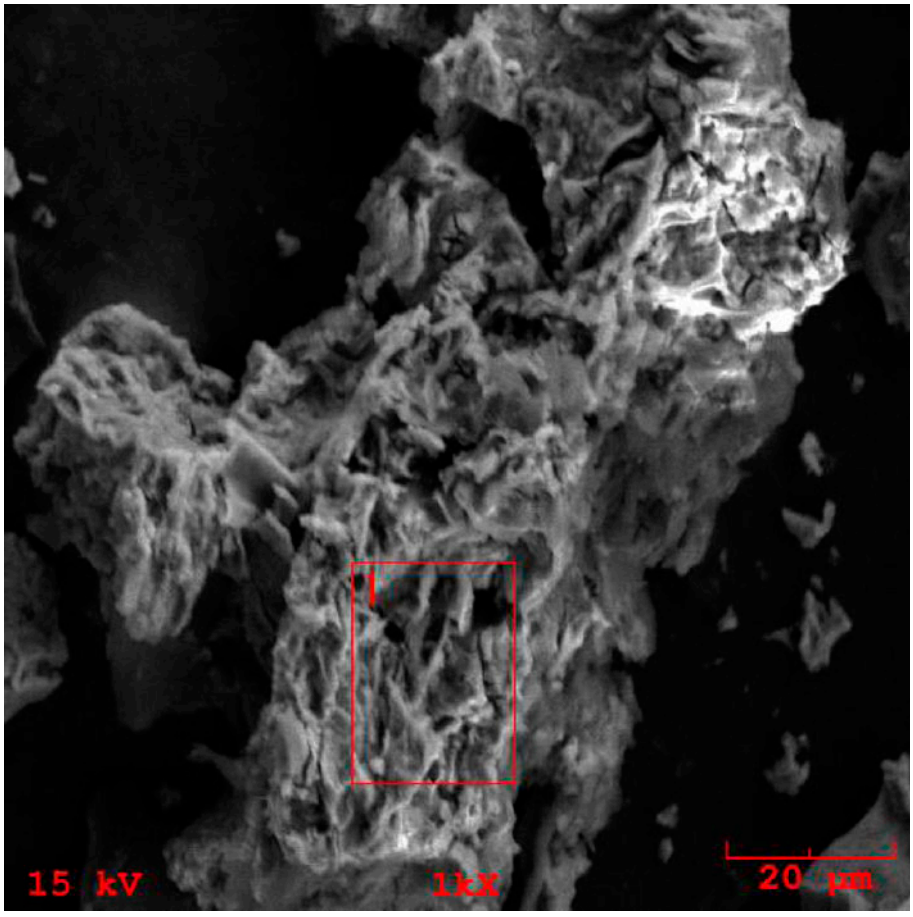

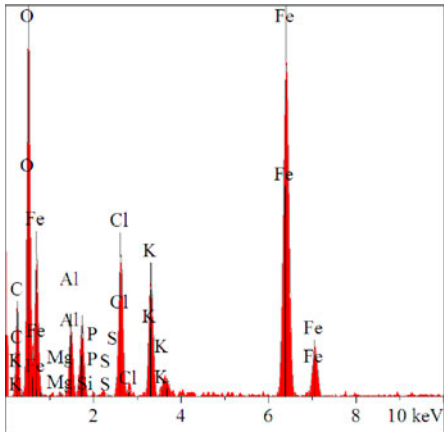

Element	Atomic %	Mass %
C	24.21	11.12
O	40.19	24.58
Fe	22.05	47.06
Total	100	100

Fig. 2. (*Continued*)

produced a large number of positive sites on the surface (Fig. 1); the protonation of surface hydroxy groups caused an increase in the electrostatic adsorption of nitrate [15]. Therefore, activation of WB with HCl can increase adsorption capacity.

The adsorption capacity and removal percentage of the adsorbents significantly improved as the amount of coated iron increased (Fig. 4(a) and Table 3). At low mass ratios (0.14 and 0.28), activation with HCl increased the adsorption capacity and removal percentage for nitrogen (Fig. 4(a) and Table 3). For example, 6HIB2 (1.00 mg g^{-1} and 23.84%) was approximately 46% higher than DIB2 (0.68 mg g^{-1} and 16.33%). However, as the ratio

(c)

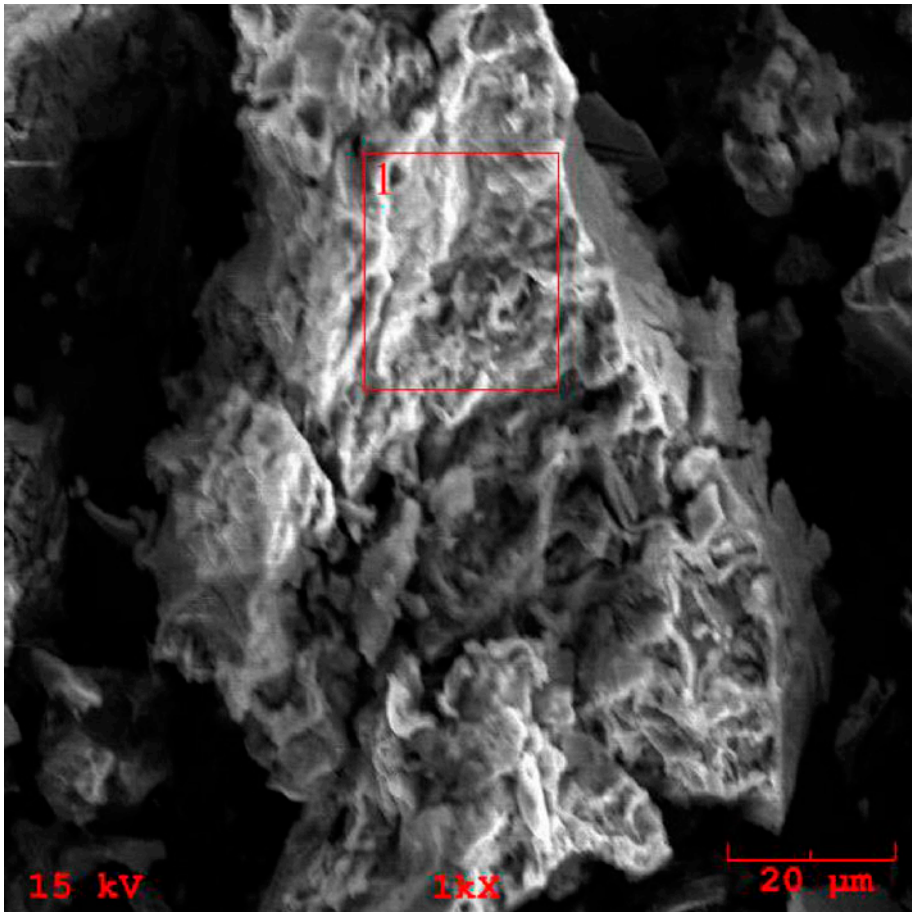

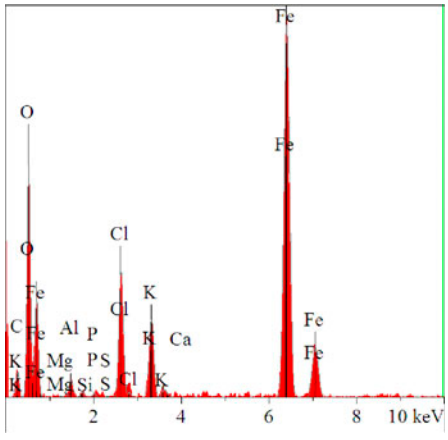

Element	Atomic %	Mass %
C	12.78	4.56
O	35.15	16.72
Fe	49.47	65.52
Total	100	100

Fig. 2. (*Continued*)

increased, the improvement caused by the HCl treatment did not continue to increase and thus, indicates that the iron coated onto the pores of DWB, 1HWB, and 6HWB was the main active position for adsorption [21].

In the three series, the adsorption capacities and removal percentages reached the maximum at a mass ratio of 0.70. This result indicates that more irons were coated onto the IB pores at this ratio than at lower mass ratios; this phenomenon resulted in more available sites for nitrate absorption. However, adsorption capacity and removal percentage began to decline at a mass ratio of 0.84 (Fig. 4(a) and Table 3) because of the decrease in the pore volume and surface area

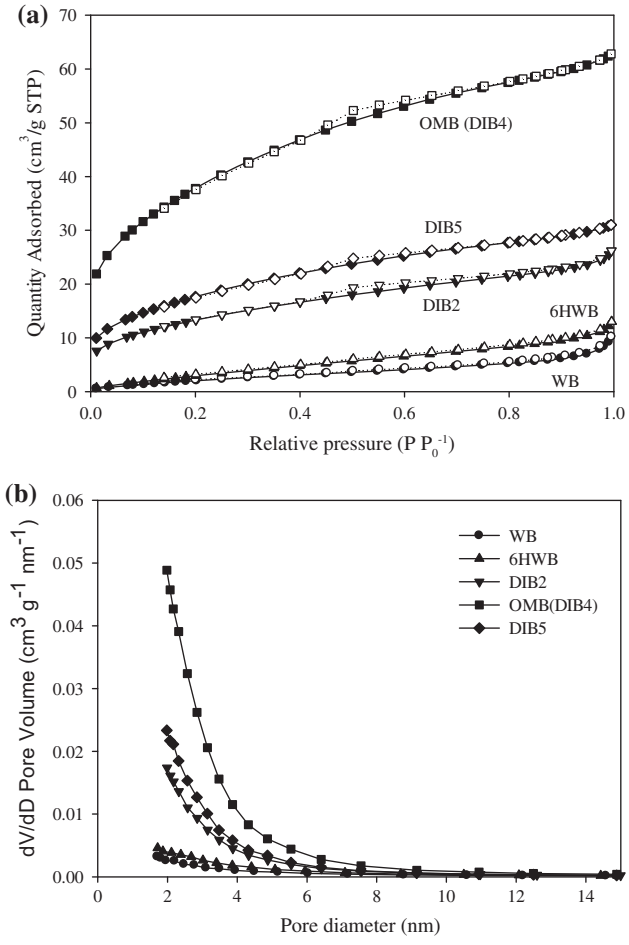

Fig. 3. N_2 adsorption (closed symbols) and desorption (open symbols) isotherms at 77 K (a) and pore size distribution (b) of WB, 6HWB, DIB2, OMB (DIB4), and DIB5.

(Table 2). This result suggests that some pores of biochar were blocked with excess iron (Fig. 2) and decreased the contact area of nitrate ions and iron (hydr)oxides. This decrease had negative effects on adsorption. The optimal ratio for nitrogen adsorption was 0.70, and no significant differences were observed among the three series at 0.70.

3.3. Phosphate adsorption

The phosphorus adsorption capacities and removal percentages of 1HWB and 6HWB were higher than those of DWB (Fig. 4(b)); approximately 74% increase was observed for 1HWB and 42% for 6HWB. These results indicate that the pores of 1HWB and 6HWB contained more activated available sites than those of DWB (Fig. 1), and the effect of treatment with HCl on the adsorption capacity and removal percentage for phosphorus was less than that of nitrogen.

The adsorption capacities and removal percentages for phosphorus of 1HWB and 6HWB were significantly lower than those of the other five 1HIBs and 6HIBs. The amount of phosphorus adsorbed and the removal percentage significantly increased as the mass ratio of iron to biochar increased (Fig. 4(b) and Table 4). A similar result was also found for the DIBs series. The effect of treatment with HCl on the adsorption capacity and removal percentage for phosphorus was very small even at low mass ratios (0.14 and 0.28) (Fig. 4(b) and Table 4). For example, 6HIB2 (7.81 mg g^{-1} and 62.89%) is only approximately 6% higher than DIB2 (7.31 mg g^{-1} and 59.52%), and both are higher than DWB (0.65 mg g^{-1} and 5.28%); these results suggest that the iron coated onto the adsorbent provided the main active positions for phosphorous adsorption [21].

The removal percentage and amount of phosphorus adsorbed onto DIB4 and DIB5 were both higher than those in DWB and exhibited no significant differences with each other. In the 1HIBs and 6HIBs, the amounts of phosphorus adsorbed and the removal percentages were not significantly different at mass

Table 2
Textural characteristics of WB, 6HWB, DIB2, DIB4, and DIB5

Samples	S_{BET} (m^2 g^{-1})	$S_{Langmuir}$ (m^2 g^{-1})	S_{BJH} (m^2 g^{-1})	V_S (cm^3 g^{-1})	V_{BJH} (cm^3 g^{-1})	D_p (nm)
WB	9.47	16.33	10.17	0.012	0.016	5.16
6HWB	14.58	26.70	15.66	0.017	0.020	4.72
DIB2	48.98	69.22	37.21	0.038	0.037	3.09
DIB4	138.56	193.97	99.77	0.095	0.084	2.75
DIB5	64.91	91.22	48.88	0.047	0.043	2.88

Notes: S_{BET}: BET surface area, $S_{Langmuir}$: Langmuir surface area, S_{BJH}: BJH adsorption cumulative surface area of pores between 1.7 and 300 nm, V_S: single point adsorption total pore volume of pores less than 75 nm in diameter, V_{BJH}: BJH adsorption cumulative volume of pores between 1.7 and 300 nm, D_p: adsorption average pore width.

Table 3
Removal percentage (%) of nitrogen from water in the three series of IBs

Mass ratio	0	0.14	0.28	0.45	0.70	0.84
DIB	0.49 ± 0.41f	10.29 ± 0.20e	16.33 ± 1.44d	25.47 ± 0.98c	37.61 ± 2.14b	32.51 ± 1.83a
1HIB	6.32 ± 0.64f	8.49 ± 0.56e	18.17 ± 1.04d	24.84 ± 1.18c	39.53 ± 0.60b	33.44 ± 3.65a
6HIB	10.59 ± 1.18d	16.12 ± 1.60c	23.84 ± 1.50b	28.11 ± 2.13b	38.97 ± 5.91a	34.72 ± 2.66a

Table 4
Removal percentage (%) of phosphorus from water in the three series of IBs

Mass ratio	0	0.14	0.28	0.45	0.70	0.84
DIB	5.28 ± 2.63e	37.89 ± 2.99d	59.52 ± 2.64c	73.98 ± 4.73b	88.63 ± 2.70a	88.50 ± 5.74a
1HIB	9.19 ± 0.44e	32.44 ± 1.27d	58.63 ± 2.65c	75.12 ± 1.10b	86.73 ± 6.49a	83.19 ± 4.01a
6HIB	7.45 ± 1.37f	40.17 ± 2.43e	62.89 ± 2.16d	79.44 ± 2.35c	86.49 ± 2.81b	92.89 ± 0.94a

ratios (iron to biochar) of 0.70 and 0.84 but were significantly higher than those in 1HIB1, 1HIB2, 1HIB3, 6HIB1, 6HIB2, and 6HIB3. This result suggests that the pores of biochar contained a large amount of iron (hydr)oxides at a high mass ratio than at a low mass ratio (Fig. 2) and thus, had more available sites for phosphate adsorption. Therefore, these types of IBs could be optimal for phosphorus adsorption.

In the three series of IBs, the phosphorus adsorption capacities of the six types of adsorbents at mass ratios (iron to biochar) of 0.70 and 0.84 were not significantly different. These results indicate that some of the biochar pores were blocked with excess iron, which led to a decrease in the active pores. This decrease may have a negative effect on the adsorption of phosphate ions onto the surface of DIB5, 1HIB5, and 6HIB5.

3.4. Determination of OMB

Biochar treatment with HCl can increase nitrogen and phosphorus adsorption capacities. However, this treatment causes production costs to increase, and results in increased environmental contamination risk. For nitrogen adsorption, no significant differences were exhibited by the three series at an iron-to-biochar mass ratio of 0.70. The phosphorus adsorption capacities of the six adsorbents at mass ratios of 0.70 and 0.84 were not significantly different. DIB4 was found to be the OMB. Therefore, the process involving DIB4 should be utilized to remove nitrogen and phosphorus pollution.

3.5. Equilibrium adsorption studies on OMB (DIB4)

The nitrogen and phosphorus adsorption capacity of DIB4 increased rapidly as the nitrate and phosphate equilibrium concentration increased. A plateau was reached eventually, which reveals that DIB4 was saturated at this level (Fig. 5). The equilibrium adsorption data were fitted through the use of Langmuir and Freundlich models. The isotherm constants are shown in Table 5.

The Langmuir isotherm [9,21–23] has been successfully applied to many adsorption processes. Its linear form is

$$\frac{C_e}{qe} = \frac{1}{bQ_0} + \frac{C_e}{Q_0} \tag{3}$$

where b is the adsorption equilibrium constant ($L\,mg^{-1}$), and Q_0 is the theoretical monolayer saturation capacity ($mg\,g^{-1}$). Table 5 shows that the correlation coefficients of nitrogen and phosphorus (R^2) are 0.987 and 0.985, respectively, and the maximum adsorption capacities (Q_0) are 2.47 mg N g^{-1} and 16.58 mg P g^{-1}, respectively.

The essential characteristics of the Langmuir isotherm can be expressed in terms of a dimensionless equilibrium parameter (R_L) [23]. The parameter is defined by

Table 5
Constants of isotherms for adsorption of nitrogen and phosphorus by DIB4

Pollutant	Langmuir			Freundlich		
	Q_0 $mg\,g^{-1}$	b $L\,mg^{-1}$	R^2	Kf	n	R^2
Nitrogen	2.47	0.11	0.987	0.3	1.77	0.991
Phosphorus	16.58	0.21	0.985	6.14	4.02	0.945

$$R_L = \frac{1}{1 + b \times C_0} \quad (4)$$

If the average of the R_L values for each of the different initial concentrations used is between 0 and 1, then positive adsorption occurs [23]. Table 5 shows that for nitrogen adsorption, b is 0.11 $L\,mg^{-1}$ and C_0 is between 5 and 50 $mg\,L^{-1}$; thus, the R_L value for nitrogen adsorption changed between 0.15 and 0.65. For phosphorus adsorption, b is 0.21 $L\,mg^{-1}$ and C_0 is between 40 and 100 $mg\,L^{-1}$; hence, the R_L value for phosphorus adsorption changed between 0.05 and 0.11. These results indicate that the adsorption behavior of DIB4 was favorable for nitrogen and phosphorus.

The Freundlich isotherm [9,21–23] is often utilized for heterogeneous surface energy systems. The Freundlich equation is expressed by the equation

$$\log qe = \log Kf + \frac{1}{n} \log C_e \quad (5)$$

where Kf and n are Freundlich constants that represent adsorption capacity and adsorption intensity, respectively. As shown in Table 5, for nitrogen adsorption, Kf is 0.32, R^2 is 0.991, and $n = 1.77$. For phosphorus adsorption, Kf is 6.14, R^2 is 0.945, and $n = 4.02$. These values of n are all larger than one and suggest that nitrate was positively adsorbed onto DIB4 [24].

3.6. Effect of initial pH on the adsorption capacity of OMB (DIB4)

When the pH of the solution increased from 3 to 11, the amount of adsorbed nitrogen decreased, but the amount of adsorbed phosphorus increased initially and then decreased (Fig. 6). The optimal pH range for nitrogen adsorption was pH 3–6, similar to phosphorus adsorption. After the final adsorption equilibrium in the two adsorption processes, the pH values of both were lower than 7 even when the initial pH of the solution was 11. The decrease in pH of the solution resulted in more protons being available to protonate the DIB4 surface, and the number of positively charged sites increased [22].

Nitrogen and phosphorus removal were most effective at pH 3 and 6, respectively, and qe was highest at 1.94 and 12.20 $mg\,g^{-1}$. Therefore, DIB4 favored acidic conditions for nitrate adsorption. For phosphorus adsorption, when the pH value was between 3 and 6, $H_2PO_4^-$ was the major species in the phosphate solution and was adsorbed onto the DIB4 surface. When the wastewater contained both nitrate and phosphate, nitrate and phosphate removal were most effective at pH 3–6.

3.7. Adsorption mechanism of OMB (DIB4)

According to the study of Saha et al. [25], akaganeite may form in the resultant OMB (DIB4); in the present study, akaganeite was formed in the ferric chloride solutions because of the interaction of chloride ions with the surface of the hydrous ion [16]. The active substance was amorphous FeOOH [25].

The Fe^{3+} ion easily forms an octahedral complex in a water solution (Fig. 7). Therefore, the structure of the hydroxylated mineral surface complex of DIB4 is similar to the Fe^{3+} ion (Fig. 7) in a water solution, where C–Fe is the surface complexes between iron (hydr)oxide and biochar.

In the adsorption process, the surface complexes formed are classified as inner- and outer-sphere complexes, depending on the bonding between the anions and surface active site [26]. In the nitrogen adsorption process, nitrate adsorption forms outer-sphere complexes through electrostatic forces as follows:

$$[C\text{–}Fe(OH_2)_5]^{3+}_{(s)} + NO^-_{3(aq)} \leftrightarrow [C - Fe(OH_2)_5]^{3+} \cdots NO^-_{3(s)} \quad (6)$$

In addition to the formed outer-sphere complexes through electrostatic forces, such as nitrate adsorption [Eqs. (7), (11), and (12)], the surface of DIB4 mainly forms the inner-complexes of ferric phosphate (Eqs. (8)–(10)) as follows:

$$[C\text{–}Fe(OH_2)_5]^{3+}_{(s)} + H_2PO^-_{4(aq)} \leftrightarrow [C - Fe(OH_2)_5]^{3+} \cdots H_2PO^-_{4(s)} \quad (7)$$

$$[C\text{–}Fe(OH_2)_5]^{3+}_{(s)} + H_2PO^-_{4(aq)} \leftrightarrow [C - Fe(OH_2)_4(H_2PO_4)]^{2+}_{(s)} + H_2O \quad (8)$$

$$[C\text{–}Fe(OH_2)_4(H_2PO_4)]^{2+}_{(s)} + H_2PO^-_{4(aq)} \leftrightarrow [C - Fe(OH_2)_3(H_2PO_4)_2]^{+} + H_2O \quad (9)$$

$$[C\text{–}Fe(OH_2)_3(H_2PO_4)_2]^{+}_{(s)} + H_2PO^-_{4(aq)} \leftrightarrow [C - Fe(OH_2)_2(H_2PO_4)_3] + H_2O \quad (10)$$

$$[C\text{–}Fe(OH_2)_4(H_2PO_4)]^{2+}_{(s)} + H_2PO^-_{4(aq)} \leftrightarrow [C - Fe(OH_2)_4(H_2PO_4)]^{2+} \cdots H_2PO^-_{4(s)} \quad (11)$$

$$[\text{C–Fe(OH}_2)_3(\text{H}_2\text{PO}_4)]^+_{(s)} + \text{H}_2\text{PO}^-_{4(aq)} \leftrightarrow [\text{C} - \text{Fe(OH}_2)_3(\text{H}_2\text{PO}_4)]^+ \cdots \text{H}_2\text{PO}^-_{4(s)} \quad (12)$$

where $H_2PO^-_{4(aq)}$ represents the main phosphate salt at pH 3–6. Iron (hydr)oxides have a high affinity for phosphate and are very selective in the adsorption process [18]. Therefore, the phosphorus adsorption capacity of DIB4 was significantly higher than its nitrogen adsorption capacity (Figs. 5 and 6).

The Fe^{3+} ion has a high charge-to-size ratio because of its high positive charge and small ion radius. This condition leads to the production of the significant hydrolytic action of Fe^{3+} in a water solution. Step-by-step hydrolytic action occurs as

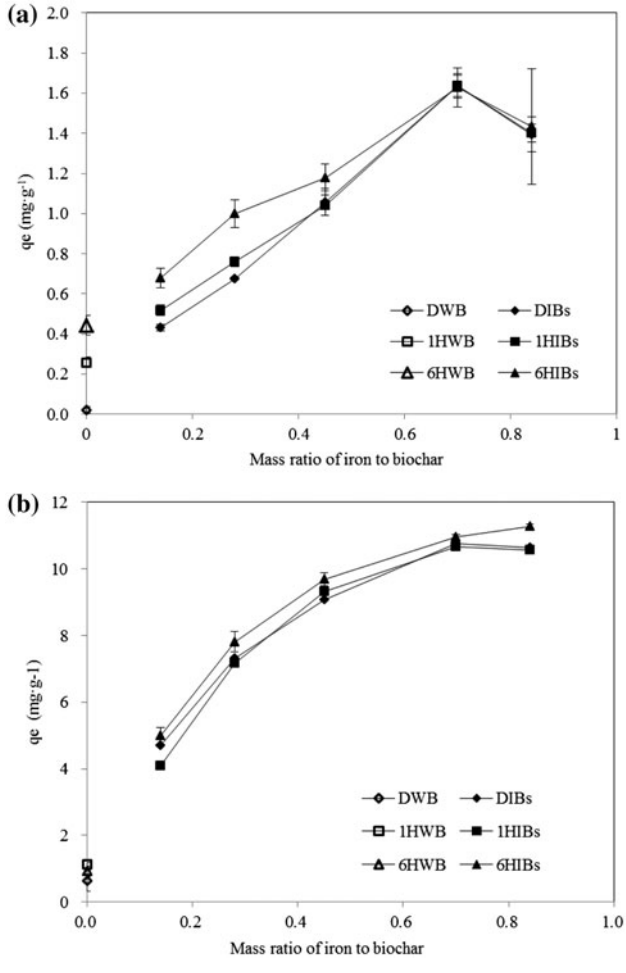

Fig. 4. Amount of nitrogen (a) and phosphorus (b) adsorbed onto DWB, 1HWB, 6HWB, DIBs, 1HIBs, and 6HIBs.

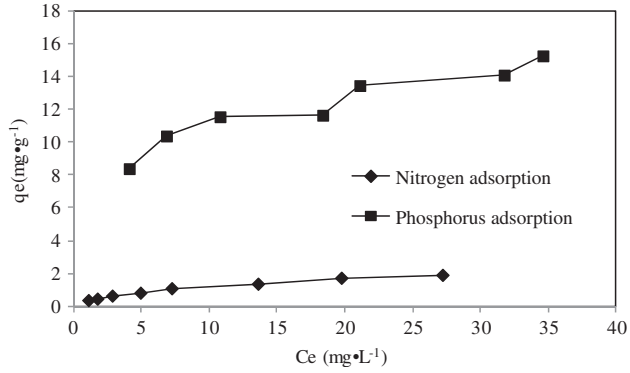

Fig. 5. Adsorption isotherms of nitrogen and phosphorus in DIB4.

$$[\text{Fe(H}_2\text{O)}_6]^{3+} + \text{H}_2\text{O} \leftrightarrow [\text{Fe(H}_2\text{O)}_5\text{(OH)}]^{2+} + \text{H}_3\text{O}^+ \quad (13)$$

$$[\text{Fe(H}_2\text{O)(OH)}]^{2+} + \text{H}_2\text{O} \leftrightarrow [\text{Fe(H}_2\text{O)}_4\text{(OH)}_2]^+ + \text{H}_3\text{O}^+ \quad (14)$$

The surface of DIB4 forms the complexes in water, similar to Eqs. (13) and (14).

$$[\text{C–Fe(OH}_2)_5]^{3+}_{(s)} + \text{H}_2\text{O} \leftrightarrow [\text{C} - \text{Fe(OH}_2)_4\text{(OH)}]^{2+}_{(s)} + \text{H}_3\text{O}^+ \quad (15)$$

$$[\text{C–Fe(OH}_2)_4\text{(OH)}]^{2+}_{(s)} + \text{H}_2\text{O} \leftrightarrow [\text{C–Fe(OH}_2)_3\text{(OH)}_2]^+_{(s)} + \text{H}_3\text{O}^+ \quad (16)$$

In the nitrogen and phosphorus solutions, a large amount of $[\text{C–Fe(OH}_2)_5]^{3+}_{(s)}$ changed into $[\text{C–Fe(OH}_2)_4\text{(OH)}]^{2+}_{(s)}$, $[\text{C–Fe(OH}_2)_3\text{(OH)}]^+_{(s)}$, and H_3O^+

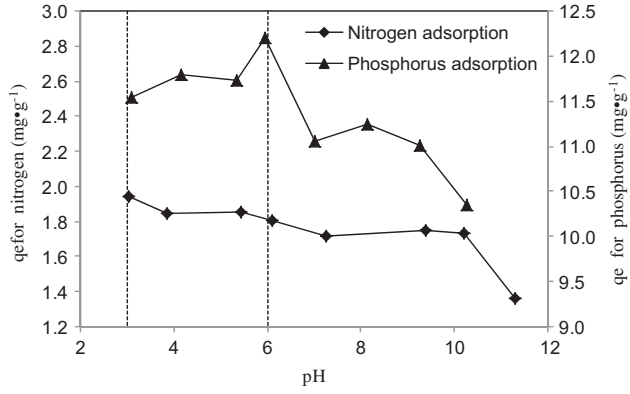

Fig. 6. Effect of pH on the nitrogen and phosphorus adsorption capacity of DIB4.

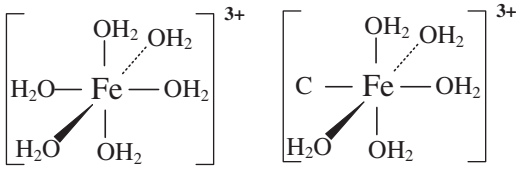

Fig. 7. Surface complexes of Fe^{3+} ion (left) and DIB4 (right) in a water solution.

[Eqs. (15) and (16)] with the increase in pH. Therefore, DIB4 had a higher nitrate and phosphate adsorption capacity in low-pH solutions than in high-pH solutions (Fig. 6). The pH of the final adsorption equilibrium solution was lower than 7 even when the initial pH of the solution was 11.

4. Conclusions

The adsorption capacity of wheat straw biochar improved significantly after coating with iron. The iron-coated biochar, DIB4, was the optimal adsorbent, and its maximum adsorption capacities were 2.47 mg N g^{-1} and 16.58 mg P g^{-1}; the most effective pH values were 3 and 6. The combination of biochar and iron maximized the increased capability of these two materials to remove nitrate and phosphate and could be an efficient means of fully utilizing wheat straw.

Acknowledgments

This research was supported by the National High-Tech R&D Program (863 Program) for the 12th Five-Year Plan (2011AA100503), the National Natural Science Foundation of China (51109214) and Technology innovation Program of Chinese Academy of Agricultural Sciences, the Agricultural Science and Technology Innovation Program (ASTIP) of Chinese Academy of Agricultural Sciences, the Special Fund for Agro-scientific Research in the Public Interest (201303095-10).

References

[1] X. Li, S. Wang, L. Duan, J. Hao, C. Li, Y. Chen, L. Yang, Particulate and trace gas emissions from open burning of wheat straw and corn stover in China, Environ. Sci. Technol. 41 (2007) 6052–6058.
[2] Y. Ding, Y.X. Liu, W.X. Wu, D.Z. Shi, M. Yang, Z.K. Zhong, Evaluation of biochar effects on nitrogen retention and leaching in multi-layered soil columns, Water Air Soil Pollut. 213 (2010) 47–55.
[3] W. Kwapinski, C.M. Byrne, E. Kryachko, P. Wolfram, C. Adley, J.J. Leahy, H.E. Novotny, M.H.B. Hayes, Biochar from biomass and waste, Waste Biomass Valor. 1 (2010) 177–189.
[4] J. Lehmann, Bio-energy in the black, Front Ecol. Environ. 5 (2007) 381–387.
[5] J. Lehmann, J. Gaunt, M. Rondon, Bio-char sequestration in terrestrial ecosystems–A review, Mitig. Adapt. Strat. Gl. Change 11 (2006) 395–419.
[6] D.A. Laird, P. Fleming, D.D. Davis, R. Horton, B. Wang, D.L. Karlen, Impact of biochar amendments on the quality of a typical Midwestern agricultural soil, Geoderma 158 (2010) 443–449.
[7] B.P. Singh, B.J. Hatton, B. Singh, A.L. Cowie, A. Kathuria, Influence of biochars on nitrous oxide emission and nitrogen leaching from two contrasting soils, J. Environ. Qual. 39 (2010) 1224–1235.
[8] S. Altenor, B. Carene, E. Emmanuel, J. Lambert, J.J. Ehrhardt, S. Gaspard, Adsorption studies of methylene blue and phenol onto vetiver roots activated carbon prepared by chemical activation, J. Hazard. Mater. 165 (2009) 1029–1039.
[9] B. Chen, Z. Chen, S. Lv, A novel magnetic biochar efficiently sorbs organic pollutants and phosphate, Bioresour. Technol. 102 (2011) 716–723.
[10] W.J. Liu, F.X. Zeng, H. Jiang, X.S. Zhang, Preparation of high adsorption capacity bio-chars from waste biomass, Bioresour. Technol. 102 (2011) 8247–8252.
[11] Y. Qiu, Z. Zheng, Z. Zhou, G.D. Sheng, Effectiveness and mechanisms of dye adsorption on a straw-based biochar, Bioresour. Technol. 100 (2009) 5348–5351.
[12] Y. Qiu, H. Cheng, C. Xu, G.D. Sheng, Surface characteristics of crop-residue-derived black carbon and lead (II) adsorption, Water Res. 42 (2008) 567–574.
[13] V. Fierro, G. Muñiz, G. Gonzalez-Sánchez, M.L. Ballinas, A. Celzard, Arsenic removal by iron-doped activated carbons prepared by ferric chloride forced hydrolysis, J. Hazard. Mater. 168 (2009) 430–437.
[14] D.K. Mahmoud, M.A.M. Salleh, W.A.W.A. Karim, A. Idris, Z.Z. Abidin, Batch adsorption of basic dye using acid treated kenaf fibre char: Equilibrium, kinetic and thermodynamic studies, Chem. Eng. J. 181 (2012) 449–457.
[15] A. Bhatnagar, M. Sillanpää, A review of emerging adsorbents for nitrate removal from water, Chem. Eng. J. 168 (2011) 493–504.
[16] M. Streat, K. Hellgardt, N.L.R. Newton, Hydrous ferric oxide as an adsorbent in water treatment: Part 1. Preparation and physical characterization, Process Saf. Environ. Prot. 86 (2008) 1–9.
[17] W. Chen, R. Parette, J. Zou, F.S. Cannon, B.A. Dempsey, Arsenic removal by iron-modified activated carbon, Water Res. 41 (2007) 1851–1858.
[18] A. Zach-Maor, R. Semiat, H. Shemer, Synthesis, performance, and modeling of immobilized nano-sized magnetite layer for phosphate removal, J. Colloid Interface Sci. 357 (2011) 440–446.
[19] Q.L. Zhang, Y.C. Lin, X. Chen, N.Y. Gao, A method for preparing ferric activated carbon composites adsorbents to remove arsenic from drinking water, J. Hazard. Mater. 148 (2007) 671–678.
[20] K.A. Krishnan, A. Haridas, Removal of phosphate from aqueous solutions and sewage using natural and surface modified coir pith, J. Hazard. Mater. 152 (2008) 527–535.
[21] X. Huang, X. Liao, B. Shi, Adsorption removal of phosphate in industrial wastewater by using

metal-loaded skin split waste, J. Hazard. Mater. 166 (2009) 1261–1265.
[22] N. Öztürk, T.E. Bektaş, Nitrate removal from aqueous solution by adsorption onto various materials, J. Hazard. Mater. B112 (2004) 155–162.
[23] I.A.W. Tan, B.H. Hameed, A.L. Ahmad, Equilibrium and kinetic studies on basic dye adsorption by oil palm fibre activated carbon, Chem. Eng. J. 127 (2007) 111–119.
[24] H. Demiral, G. Gündüzoğlu, Removal of nitrate from aqueous solutions by activated carbon prepared from sugar beet bagasse, Bioresour. Technol. 101 (2010) 1675–1680.
[25] B. Saha, R. Bains, F. Greenwood, Physicochemical characterization of granular ferric hydroxide (GFH) for arsenic(V) sorption from water, Sep. Sci. Technol. 40 (2005) 2909–2932.
[26] C. Namasivayam, K. Prathap, Recycling Fe(III)/Cr(III) hydroxide, an industrial solid waste for the removal of phosphate from water, J. Hazard. Mater. B123 (2005) 127–134.